Temperature-controllable spin-polarized current and spin polarization in a Rashba three-terminal double-quantum-dot device*

Hong Xue-Kun(洪学鹃), Yang Xi-Feng(杨希峰), Feng Jin-Fu(冯金福), and Liu Yu-Shen(刘玉申)†

Laboratory of Advanced Functional Materials and College of Physics and Engineering, Changshu Institute of Technology, Changshu 215500, *China*

(Received 17 October 2012; revised manuscript received 26 November 2012)

We propose a Rashba three-terminal double-quantum-dot device to generate a spin-polarized current and manipulate the electron spin in each quantum dot by utilizing the temperature gradient instead of the electric bias voltage. This device possesses a nonresonant tunneling channel and two resonant tunneling channels. The Keldysh nonequilibrium Green's function techniques are employed to determinate the spin-polarized current flowing from the electrodes and the spin accumulation in each quantum dot. We find that their signs and magnitudes are well controllable by the gate voltage or the temperature gradient. This result is attributed to the change in the slope of the transmission probability at the Fermi levels in the low-temperature region. Importantly, an obviously pure spin current can be injected into or extracted from one of the three electrodes by properly choosing the temperature gradient and the gate voltages. Therefore, the device can be used as an ideal thermal generator to produce a pure spin current and manipulate the electron spin in the quantum dot.

Keywords: Rashba quantum dot, spin polarization, spin accumulation, temperature gradient

PACS: 73.63.Kv, 71.70.Ej, 72.20.Pa **DOI:** 10.1088/1674-1056/22/5/057306

1. Introduction

The advances in the nanofabrication of solid-state quantum devices have inspired extensively theoretical and experimental investigations on the electronic transport through nanoscale systems in recent years. Particular interest has been focused on the transport properties of quantum dots (QDs) attached to metallic electrodes via tunneling barriers.[1] When an electric bias is applied across these systems, electrons or holes can move along a certain direction; thus, an electric current is generated. As is known to all, electrons or holes carry not only the electric charge but also the spin. How to generate a spin-polarized current in a controllable way in semiconductor nanostructures has attracted wide attention due to its potential applications in modern spintronics.[2] Up to now, some effective methods have been proposed. For example, the primary techniques mainly rely on optical techniques or magnetic materials.[3,4] In 1990, Datta and Das proposed a spin transistor and demonstrated the possibility of controlling the electron spin degree of freedom based on the Rashba spin–orbit interaction (RSOI).[5] The RSOI originates from the inversion asymmetry of the electric field in a two-dimensional electron system, and provides an alternative way to manipulate the spin degree of freedom.[6,7] Many recent theoretical and experimental studies show that the spin polarization can reach as high as 100%.[8–14] Another important subject in modern spintronics is the spin-dependent quantum interference phenomena. When the spin-up and spin-down electrons move through semiconductor nanostructures with the RSOI, a spin-dependent quantum interference effect occurs. Some interesting quantum phase coherence phenomena emerge. For instance, Sánchez *et al*. predicted the occurrence of a Fano-line shape in a semiconductor quantum wire in the presence of a local RSOI, which was referred to as the Fano–Rashba effect.[15] Chen *et al*. investigated the spin-dependent quantum interference effects and the spin accumulation on double quantum dots with the Rashba spin–orbit coupling and the electron–electron interaction. The result showed that the magnitude and the direction of the spin polarization are controlled by the dot levels.[16]

The research on multi-terminal devices in mesoscopic physics dates back to the early 1980s.[17–19] In comparison with the usual two-terminal electrode geometry, more useful applications and information can be extracted in the devices with a three-terminal electrode geometry. For example, a direct measure of the electron–hole asymmetry of the quantum dot system can be achieved.[20] When the QD is in the Kondo regime, the differential conductance is suppressed at zero bias.[21] Furthermore, there has been some recent work focusing on the spin-polarized currents driven by an electric bias in a three-terminal ring-like structure involving a single-level Rashba QD. The spin-up and spin-down electrons from one electrode can be completely separated by the QD, and injected into the other two electrodes, respectively.[10]

In addition to the electric fields, temperature fields can

*Project supported by the National Natural Science Foundation of China (Grant Nos. 11247028, 11147162, and 61106126) and the Open Fund of Jiangsu Laboratory of Advanced Functional Materials, China (Grant No. 12KFJJ001).

†Corresponding author. E-mail: ysliu@cslg.edu.cn

© 2013 Chinese Physical Society and IOP Publishing Ltd

also drive electrons or holes to move along a certain direction, and thus a temperature-bias-induced current can be generated. Such an effect is called the Seebeck effect, which has been widely investigated in QD and molecular systems.[22–28] The strength of the Seebeck effect can be characterized by the Seebeck coefficient. In coherent tunneling regions, it is related not only to the magnitude but also to the slope of the transmission function at the Fermi levels. So the Seebeck coefficient can provide more information than the current–voltage characteristics. The first experimental observation of the spin Seebeck effect in the permalloy (NiFe) has been reported by detecting the redistribution of the electron spin along the sample's longitudinal direction.[29] That experimental finding has inspired extensively experimental[30,31] and theoretical[32,33] investigations in various systems. The heat-to-spin discovery can be named as thermo-spintronics. In spite of the large amount of theoretical work on the spin-dependent thermoelectric effects in a single QD or double QDs attached to ferromagnetic leads with collinear or noncollinear magnetic moments, almost all the attention has been focused only on the two-terminal geometry so far.[34–43]

In this paper, we shall show how to generate a spin-polarized current and manipulate the electron spin in QDs by utilizing the temperature gradient instead of the voltage bias in a Rashba three-terminal double-quantum-dot device. The device, which is schematically shown in Fig. 1, consists of three metallic electrodes separated by two QDs with intra-dot Coulomb interactions. The QDs are realized in the two-dimensional electron gas of an AlGaAs/GaAs heterostructure.[44] A nonresonant tunneling channel between the right electrodes is presented. The temperature-induced spin-polarized current through the electrodes and the spin accumulation on the QDs are calculated within the Keldysh nonequilibrium Green's function formalism. Unlike the voltage-induced current related to the sum of the transmission probabilities in the voltage-bias window, the temperature-induced current is determined by the slope of the transmission probability at the Fermi levels. Therefore, the transport direction of the spin-polarized current is sensitive to the location of the intra-dot energy levels with respect to the Fermi levels. The positive and the negative maxima of the spin-polarized currents and the spin accumulation emerge separately at the two sides of the Coulomb peaks. Their directions can be easily controlled by the gate voltage or the temperature of the electrodes. Importantly, the temperature-induced spin-polarization efficiency through the electrodes can approach 100% (−100%) or even infinity, which means that a pure spin-up (spin-down) current or a pure spin current can be generated by the present device.

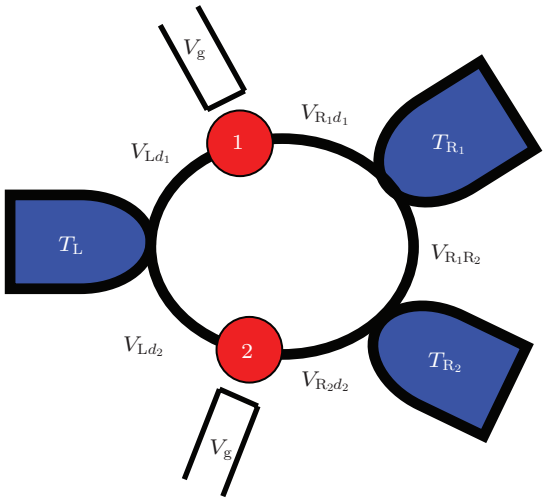


Fig. 1. (color online) Schematic diagram of a ring-shaped device. The three metallic electrodes serve as the temperature reservoirs with temperatures T_L and T_{R_n} $(n = 1,2)$, respectively. The two red filled-in circles represent the 1st and the 2nd QDs, respectively. The intra-dot energy level on each QD can be tuned by gate voltage V_g.

2. Model and method

We write the Hamiltonian of the device in the form

$$\mathscr{H} = \mathscr{H}_E + \mathscr{H}_D + \mathscr{H}_T, \tag{1}$$

where

$$\mathscr{H}_E = \sum_{k,\sigma,\alpha=L,R_j(j=1,2)} \varepsilon_{\alpha k} c^\dagger_{\alpha k\sigma} c_{\alpha k\sigma} \tag{2}$$

describes three isolated electrodes indexed by α, in which the electrons are free from the interaction except for an overall self-consistent potential. Here $c^\dagger_{\alpha k\sigma}$ $(c_{\alpha k\sigma})$ is the creation (annihilation) operator of an electron with spin $\sigma = \uparrow,\downarrow$ (or $\sigma = 1,-1$) and energy $\varepsilon_{\alpha k}$ in electrode α. The Hamiltonian of the two QDs, $\mathscr{H}_D$, is given by

$$\mathscr{H}_D = \sum_{j,\sigma} \varepsilon_j d^\dagger_{j\sigma} d_{j\sigma} + \sum_j U_j d^\dagger_{j\uparrow} d_{j\uparrow} d^\dagger_{j\downarrow} d_{j\downarrow}, \tag{3}$$

where ε_j is the bare energy level, and U_j is the intra-dot Coulomb interaction on each QD. The operator $d^\dagger_{j\sigma}$ $(d_{j\sigma})$ creates (destroys) an electron with spin σ on the j-th QD, where the intra-dot energy level can be well controlled by the gate voltage (see Fig. 1). The tunneling process $\mathscr{H}_T$ in Eq. (1) includes two parts: (i) one is the tunnel coupling between the right two electrodes (a nonresonant tunneling channel); (ii) the other is the tunnel couplings between the electrodes and the central QD region (two resonant tunneling channels). Thus we write the total tunneling Hamiltonian as

$$\begin{aligned}\mathscr{H}_T =& \sum_{k,\sigma} (V_{R_1R_2} e^{-i\sigma\varphi_R} c^\dagger_{R_1k\sigma} c_{R_2k\sigma} + \text{H.c.}) \\ &+ \sum_{k,\sigma,j} (V_{R_jd_j} c^\dagger_{R_jk\sigma} d_{j\sigma} + \text{H.c.}) \\ &+ \sum_{k,\sigma,j} (V_{Ld_j} c^\dagger_{Lk\sigma} d_{j\sigma} + \text{H.c.}),\end{aligned} \tag{4}$$

where parameter $V_{\alpha d_j}$ represents the tunnel coupling strength between the electrodes and the center QD region. An extra spin-dependent phase factor $e^{-i\sigma\varphi_R}$ has been added into the tunnel coupling strength $V_{R_1R_2}$, which arises from the RSOI on the QD. Here we have assumed that the RSOI only exists inside the QDs, which will arouse two main effects. One is a phase factor in the tunnel elements, the other is an interlevel spin-flip term. Since only one energy level in each QD is considered, we can neglect the latter term.[45] The magnitude of φ_R can reach $\pi/2$ in some semiconductors.[46,47]

When temperature gradients among the three electrodes are presented, the electrons can tunnel from one electrode through resonant or nonresonant tunneling channels into another electrode. In steady states, an electric current can be obtained. After considering the spin degree of freedom in nonequilibrium cases, we can calculate the spin-dependent electric current flowing into the center region from electrode α by using the time evolution of the occupation number operator of electrode α [48]

$$J_{\alpha\sigma} = -e\left\langle \frac{d\hat{N}_{\alpha\sigma}}{dt} \right\rangle = -\frac{ie}{\hbar}\langle[\mathscr{H}_T, \hat{N}_{\alpha\sigma}]\rangle, \tag{5}$$

where $\hat{N}_{\alpha\sigma} = \sum_k c^\dagger_{\alpha k\sigma} c_{\alpha k\sigma}$, e is the absolute electric charge, and $\hbar$ is the reduced Planck constant. Since both $\mathscr{H}_E$ and $\mathscr{H}_D$ commute with $\hat{N}_{\alpha\sigma}$, only $\mathscr{H}_T$ is left. After a little algebra, we readily obtain the spin-dependent electric current flowing out of the electrodes by lesser Green's functions in the ε representation

$$\begin{aligned} J_{L\sigma} &= \frac{2e}{\hbar}\int\frac{d\varepsilon}{2\pi}\mathrm{Re}[V_{Ld_1}G^<_{d_1L\sigma}(\varepsilon) + V_{Ld_2}G^<_{d_2L\sigma}(\varepsilon)], \quad (6)\\ J_{R_{1(2)}\sigma} &= \frac{2e}{\hbar}\int\frac{d\varepsilon}{2\pi}\mathrm{Re}[V_{R_{1(2)}d_{1(2)}}G^<_{d_{1(2)}R_{1(2)}\sigma}(\varepsilon) \\ &\quad + V_{R_1R_2}e^{\mp i\sigma\varphi_R}G^<_{R_{2(1)}R_{1(2)}\sigma}(\varepsilon)], \end{aligned} \tag{7}$$

where $G^<_{d_j\alpha\sigma}(\varepsilon)$ and $G^<_{\alpha'\alpha\sigma}(\varepsilon)$ are the Fourier transforms of the time-dependent lesser Green's functions $G^<_{d_n\alpha\sigma}(t,t') \equiv i\langle\sum_k c^\dagger_{\alpha k\sigma}(t')d_{n\sigma}(t)\rangle$ and $G^<_{\alpha'\alpha\sigma}(t,t') \equiv i\langle\sum_k c^\dagger_{\alpha k\sigma}(t')\sum_{k'} c_{\alpha' k'\sigma}(t)\rangle$, respectively. To calculate the electric current induced by the temperature gradient, we need to know the spin-dependent lesser Green's functions. Following the procedure in Ref. [45], we write all spin-dependent lesser Green's functions in the form of 5×5 matrix $\boldsymbol{G}^<_\sigma(\varepsilon)$. The corresponding retarded and advanced Green's functions are symbolized by $\boldsymbol{G}^r_\sigma(\varepsilon)$ and $\boldsymbol{G}^a_\sigma(\varepsilon)$, respectively. The retarded (advanced) Green's function $\boldsymbol{G}^{r(a)}_\sigma(\varepsilon)$ is the Fourier transform of the two-time Green's function $\boldsymbol{G}^{r(a)}_\sigma(t,t')$, and is defined as $G^{r(a)}_{\alpha\alpha'\sigma}(t,t') = \mp i\theta(\pm t\mp t')\langle\{\sum_k c_{k\alpha\sigma}(t), \sum_{k'} c^\dagger_{k'\alpha'\sigma}(t')\}\rangle$, where $\theta(\pm t\mp t')$ is the step function. There is a similar definition for Green's function $G^{r(a)}_{d_j\alpha}(t,t')$. In the case of noninteracting electrodes, $\boldsymbol{G}^<_\sigma(\varepsilon)$ is calculated by the Keldysh equation

$$\boldsymbol{G}^<_\sigma(\varepsilon) = \boldsymbol{G}^r_\sigma(\varepsilon)\boldsymbol{\Sigma}^<_\sigma(\varepsilon)\boldsymbol{G}^a_\sigma(\varepsilon), \tag{8}$$

where the retarded (advanced) Green's function $\boldsymbol{G}^{r(a)}_\sigma(\varepsilon)$ is the Fourier transformation of $\boldsymbol{G}^{r(a)}_\sigma(t,t')$, and $\boldsymbol{G}^r_\sigma(\varepsilon)$ is obtained by the Dyson equation

$$\boldsymbol{G}^r_\sigma(\varepsilon) = \boldsymbol{g}^r_\sigma(\varepsilon) + \boldsymbol{g}^r_\sigma(\varepsilon)\boldsymbol{\Sigma}^r_\sigma(\varepsilon)\boldsymbol{G}^r_\sigma(\varepsilon). \tag{9}$$

The $\boldsymbol{\Sigma}^<_\sigma(\varepsilon)$ in Eq. (8) is the noninteracting tunneling lesser self-energy, and $\boldsymbol{\Sigma}^r_\sigma(\varepsilon)$ in Eq. (9) is the corresponding retarded self-energy. In the present case, $\boldsymbol{G}^r_\sigma$ has a 5×5 matrix form

$$\boldsymbol{G}^r_\sigma(\varepsilon) = \begin{pmatrix} G^r_{R_1R_1\sigma}(\varepsilon) & G^r_{R_1L\sigma}(\varepsilon) & G^r_{R_1R_2\sigma}(\varepsilon) & G^r_{R_1d_1\sigma}(\varepsilon) & G^r_{R_1d_2\sigma}(\varepsilon) \\ G^r_{LR_1\sigma}(\varepsilon) & G^r_{LL\sigma}(\varepsilon) & G^r_{LR_2\sigma}(\varepsilon) & G^r_{Ld_1\sigma}(\varepsilon) & G^r_{Ld_2\sigma}(\varepsilon) \\ G^r_{R_2R_1\sigma}(\varepsilon) & G^r_{R_2L\sigma}(\varepsilon) & G^r_{R_2R_2\sigma}(\varepsilon) & G^r_{R_2d_1\sigma}(\varepsilon) & G^r_{R_2d_2\sigma}(\varepsilon) \\ G^r_{d_1R_1\sigma}(\varepsilon) & G^r_{d_1L\sigma}(\varepsilon) & G^r_{d_1R_2\sigma}(\varepsilon) & G^r_{d_1d_1\sigma}(\varepsilon) & G^r_{d_1d_2\sigma}(\varepsilon) \\ G^r_{d_2R_1\sigma}(\varepsilon) & G^r_{d_2L\sigma}(\varepsilon) & G^r_{d_2R_2\sigma}(\varepsilon) & G^r_{d_2d_1\sigma}(\varepsilon) & G^r_{d_2d_2\sigma}(\varepsilon) \end{pmatrix}. \tag{10}$$

The advanced Green's function $\boldsymbol{G}^a_\sigma(\varepsilon)$ can be obtained by $\boldsymbol{G}^a_\sigma(\varepsilon) = [\boldsymbol{G}^r_\sigma(\varepsilon)]^\dagger$. The $\boldsymbol{g}^r_\sigma(\varepsilon)$ is the retarded Green's function of the isolated QDs, and only the diagonal elements of $\boldsymbol{g}^r_\sigma(\varepsilon)$ are nonzero. Under the wide-band approximation, $g^r_{\alpha\alpha\sigma}(\varepsilon)$ for the electrodes has the expression $g^r_{\alpha\alpha\sigma}(\varepsilon) = -i\pi\rho_\alpha$, where ρ_α is the local density of states (LDOS) in electrode α. The $g^r_{d_jd_j\sigma}(\varepsilon)$ of the isolated j-th QD is calculated by

$$g^r_{d_jd_j\sigma}(\varepsilon) = \frac{1-\langle n_{j\bar\sigma}\rangle}{\varepsilon-\varepsilon_j} + \frac{\langle n_{j\bar\sigma}\rangle}{\varepsilon-\varepsilon_j-U_j}, \tag{11}$$

where $\langle n_{j\bar\sigma}\rangle$ is the occupation number with spin $\bar\sigma$ on the j-th QD ($\bar\sigma = -\sigma$), and is obtained by the self-consistent equation

$$\langle n_{j\bar\sigma}\rangle = -i\int\frac{d\varepsilon}{2\pi}G^<_{d_jd_j\bar\sigma}(\varepsilon). \tag{12}$$

Equation (11) clearly shows two resonances centered in the vicinities of ε_j and ε_j+U_j with the weights $(1-\langle n_{j\bar\sigma}\rangle)$ and $\langle n_{j\bar\sigma}\rangle$, respectively. By choosing a suitable noninteracting tunneling retarded self-energy, we write $\boldsymbol{\Sigma}^r_\sigma(\varepsilon)$ in the Dyson equation as[45]

$$\boldsymbol{\Sigma}^{\rm r}_{\sigma}(\varepsilon)=\begin{pmatrix} 0 & 0 & V_{\rm R_1R_2}\,{\rm e}^{-{\rm i}\sigma\varphi_{\rm R}} & V_{\rm R_1}d_1 & 0 \\ 0 & 0 & 0 & V_{\rm L}d_1 & V_{\rm L}d_2 \\ V_{\rm R_1R_2}\,{\rm e}^{{\rm i}\sigma\varphi_{\rm R}} & 0 & 0 & 0 & V_{\rm R_2}d_2 \\ V_{\rm L_1}d_1 & V_{\rm R_1}d_1 & 0 & 0 & 0 \\ 0 & V_{\rm L}d_2 & V_{\rm R_2}d_2 & 0 & 0 \end{pmatrix}. \tag{13}$$

For the sake of simplicity, we only consider the elastic scattering in the present case. The spin-dependent lesser self-energy in Eq. (8) can be obtained by $\boldsymbol{\Sigma}^{<}_{\alpha'\alpha\sigma}=2{\rm i}\delta_{\alpha\alpha'}f_{\alpha}(\varepsilon)/(\pi\rho_{\alpha})$, and $\Sigma^{<}_{d_jd_j\sigma}=0$. Here $f_{\alpha}(\varepsilon)=1/\{1+\exp[(\varepsilon-\mu_{\alpha})/k_{\rm B}T_{\alpha}]\}$ is the Fermi–Dirac distribution function in electrode α, where μ_{α} is the chemical potential, T_{α} is the temperature of electrode α, and $k_{\rm B}$ is the Boltzmann's constant. Using Eq. (8), we write all the lesser Green's functions appearing in Eqs. (6) and (7) as

$$G^{<}_{d_j\alpha\sigma}(\varepsilon)=\sum_{\alpha'}G^{\rm r}_{d_j\alpha'\sigma}(\varepsilon)\Sigma^{<}_{\alpha'\alpha'\sigma}(\varepsilon)G^{\rm a}_{\alpha'\alpha\sigma}(\varepsilon), \tag{14}$$

$$G^{<}_{\alpha\alpha'\sigma}(\varepsilon)=\sum_{\alpha''}G^{\rm r}_{\alpha\alpha''\sigma}(\varepsilon)\Sigma^{<}_{\alpha''\alpha''\sigma}(\varepsilon)G^{\rm a}_{\alpha''\alpha\sigma}(\varepsilon). \tag{15}$$

To gain more insight into how the electrons transport in the present device, we introduce a series of spin-dependent electronic transmission probabilities with different physical meanings

$$\tau_{\alpha\alpha'd_j\sigma}(\varepsilon)=-\frac{4}{\pi\rho_{\alpha'}}{\rm Im}[V_{\alpha d_j}G^{\rm r}_{d_j\alpha'\sigma}(\varepsilon)G^{\rm a}_{\alpha'\alpha\sigma}(\varepsilon)], \tag{16}$$

$$\tau_{\alpha\alpha'\alpha''\sigma}(\varepsilon)=-\frac{4}{\pi\rho_{\alpha'}}{\rm Im}[V_{\alpha\alpha''}\,{\rm e}^{\mp{\rm i}\sigma\varphi_{\rm R}}G^{\rm r}_{\alpha\alpha'\sigma}(\varepsilon)G^{\rm a}_{\alpha'\alpha''\sigma}(\varepsilon)]. \tag{17}$$

For the above two definitions, we need to make some further explanations. In Eq. (16), when $\alpha\neq\alpha'$, $\tau_{\alpha\alpha'd_j\sigma}(\varepsilon)$ represents the electronic transmission probability of the electron with spin index σ and energy ε from electrode α' to electrode α via the j-th QD. If $\alpha=\alpha'$, it is the electronic transmission probability from electrode α to the j-th QD. Similar meanings are given by Eq. (17), while we need to note that the values of α and α'' are restricted to $\rm R_1$ and $\rm R_2$. The reason is that only the nonresonant tunnel coupling between the right two electrodes is considered (see Fig. 1). The sign of the phase factor from the RSOI in Eq. (17) is dependent on the orders of α and α''. For example, the sign is negative for $\alpha=\rm R_1$ and $\alpha''=\rm R_2$, and it becomes positive when $\alpha=\rm R_2$ and $\alpha''=\rm R_1$. Substituting Eqs. (16) and (17) into Eqs. (6) and (7), we obtain

$$J_{\rm L\sigma}=\frac{e}{h}\int{\rm d}\varepsilon\sum_{\alpha=L,{\rm R}_{1(2)}}f_{\alpha}(\varepsilon)[\tau_{\rm L\alpha d_1\sigma}(\varepsilon)+\tau_{\rm L\alpha d_2\sigma}(\varepsilon)], \tag{18}$$

$$J_{\rm R_1\sigma}=\frac{e}{h}\int{\rm d}\varepsilon\sum_{\alpha=L,{\rm R}_{1(2)}}f_{\alpha}(\varepsilon)[\tau_{\rm R_{1(2)}\alpha d_{1(2)}\sigma}(\varepsilon)+\tau_{\rm R_{1(2)}\alpha R_{2(1)}\sigma}(\varepsilon)]. \tag{19}$$

For each electrode, we should note that the total electronic transmission probability into and out of each electrode is conservative, namely, $\sum_{\alpha=\rm L,R_{1(2)}}[\tau_{\rm L\alpha d_1\sigma}(\varepsilon)+\tau_{\rm L\alpha d_2\sigma}(\varepsilon)]=0$ and $\sum_{\alpha}[\tau_{\rm R_{1(2)}\alpha d_{1(2)}\sigma}(\varepsilon)+\tau_{\rm R_{1(2)}\alpha R_{2(1)}\sigma}(\varepsilon)]=0$. We also need to note that the electronic transmission probability is negative if electrons enter into the electrodes, while it is positive for electrons flowing out of the electrodes. Thus we arrive at

$$J_{\rm L\sigma}=\frac{e}{h}\int{\rm d}\varepsilon\sum_{\alpha=\rm R_1,R_2}[f_{\alpha}(\varepsilon)-f_{\rm L}(\varepsilon)]\times[\tau_{\rm L\alpha d_1\sigma}(\varepsilon)+\tau_{\rm L\alpha d_2\sigma}(\varepsilon)], \tag{20}$$

$$J_{\rm R_{1(2)}\sigma}=\frac{e}{h}\int{\rm d}\varepsilon\sum_{\alpha=\rm R_{2(1)},L}[f_{\alpha}(\varepsilon)-f_{\rm R_{1(2)}}(\varepsilon)]\times[\tau_{\rm R_{1(2)}\alpha d_{1(2)}\sigma}(\varepsilon)+\tau_{\rm R_{1(2)}\alpha R_{2(1)}\sigma}(\varepsilon)]. \tag{21}$$

The above compact equations clearly show the relations between the electric currents and the transmission probabilities.

3. Results and discussion

In this section, we present the numerical results and discussion. First, we set some parameters used in the numerical calculations. The tunnel coupling strengths in the dot–electrode and the electrode–electrode have an identical magnitude $V_{{\rm L}d_n}=V_{{\rm R}d_n}=V_{\rm R_1R_2}=V=0.4$, and thus the corresponding linewidth function $\Gamma=2\pi\rho|V_{\alpha d_n}|^2\simeq 1$ is set to be the energy unit. For the sake of simplicity, the same intra-dot Coulomb interactions and energy levels on the QDs are considered, i.e., $U_j=U$ and $\varepsilon_j=\varepsilon_d$. All the chemical potentials are independent of the temperatures of the electrodes ($\mu_{\alpha}=\mu=0$). Such an assumption is reasonable when the electrodes are large enough and the temperatures of the electrodes are not too high.

To demonstrate the physical meanings of the electronic transmission probabilities, we first consider a simple case in the absence of the temperature gradients, the RSOI, and the inter-electrode coupling between the right two electrodes, and thus all the electronic transmission probabilities are spin-independent. The negative electronic transmission probability means the electrons flowing into the electrodes, and the positive one represents the electrons flowing out of the electrodes. As electrodes $\rm R_1$ and $\rm R_2$ lie in the same state, we only plot the result for electrode $\rm R_1$. The intra-dot Coulomb interaction on each QD induces two peaks in the in-transmission spectrum. One is centered at ε_d, and the other is at ε_d+U. From top to bottom, figure 2 shows the contributions to the electronic

transmission probabilities through electrodes L (left column) and R_1 (right column) from electrodes R_1, L, and R_2. Figure 2(a) displays the electron transmission probability from electrode R_1 to electrode L, and less electrons from electrode L into the second QD ($|\tau_{LR_1d_1\sigma}| > |\tau_{LR_1d_2\sigma}|$). Figure 2(b) shows the transmission probability from electrode L, and we have $\tau_{LLd_1\sigma} = \tau_{LLd_2\sigma}$. This result means that the electrons from electrode L have the same probability entering into the two QDs, which is reasonable (see the inset of Fig. 2(b)). A similar analysis can be employed to the other figures of Fig. 2. For electrode R_1, it is worth noting that the electronic transmission probability $\tau_{R_1R_\alpha R_2}$ is zero due to $V_{R_1R_2} = 0$. These numerical results also clearly show that the electronic transmission probabilities through the electrodes satisfy the conservation laws $\sum_{\alpha=L,R_{1(2)}}[\tau_{L\alpha d_1\sigma}(\varepsilon) + \tau_{L\alpha d_2\sigma}(\varepsilon)] = 0$ (left electrode) and $\sum_\alpha[\tau_{R_{1(2)}\alpha d_{1(2)}\sigma}(\varepsilon) + \tau_{R_{1(2)}\alpha R_{2(1)}\sigma}(\varepsilon)] = 0$ (right two electrodes).

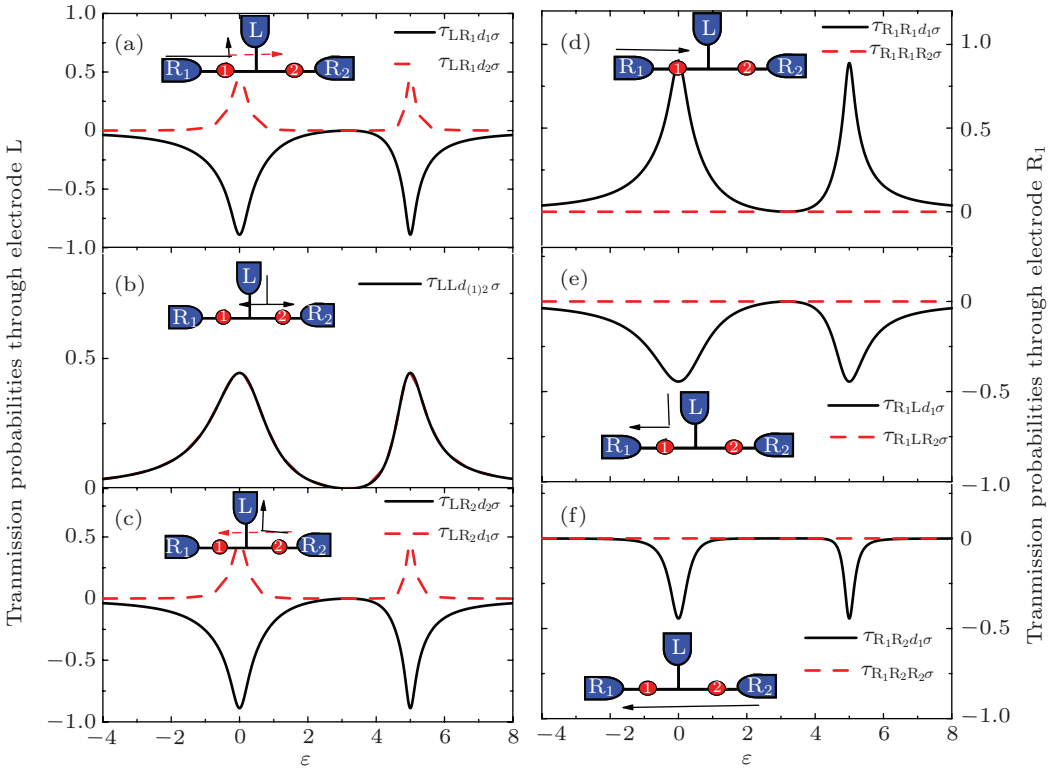


Fig. 2. (color online) Electronic transmission probabilities through electrodes ((a)–(c)) L ((d)–(f)) and R_1 as functions of the incident electron energy. The other parameters are $U = 5$ and $\varepsilon_d = 0$.

Now we show how to generate a spin-polarized current in the Rashba three-terminal double-quantum-dot device. We first give a physical interpretation of the generation of the spin polarization and the spin accumulation in the device. When an electric bias (or a thermal bias) is applied across the device, the electron will propagate from one electrode to another electrode. For example, there are two paths when the electron flows from electrode L to electrode R_1. One path is through the 1st QD to electrode R_1, and the other path is first traveling to the 2nd QD and through electrode R_2 and then into electrode R_1. If the RSOI is considered, the electrons with different spin indexes along different paths often pick up different phases. This fact results in a spin-dependent quantum interference effect. Thus when the device is in a nonequilibrium state, the spin polarization and the spin accumulation in the device are generated. The temperature of the left electrode is raised by ΔT from T ($T_L = T + \Delta T$), and those of the right two electrodes are fixed at T ($T_{R_{1(2)}} = T$). In this case, the three-terminal structure degenerates into a two-terminal one. Equations (20) and (21) reduce to

$$J_{L\sigma} = \frac{e}{h}\int d\varepsilon[f_R(\varepsilon) - f_L(\varepsilon)][\tau_{LR_1\sigma}(\varepsilon) + \tau_{LR_2\sigma}(\varepsilon)], \quad (22)$$

$$J_{R_{1(2)}\sigma} = \frac{e}{h}\int d\varepsilon[f_L(\varepsilon) - f_R(\varepsilon)]\tau_{LR_{1(2)}\sigma}, \quad (23)$$

where we have defined $f_R = f_{R_{1(2)}}$, $\tau_{R_{1(2)}L\sigma}(\varepsilon) = \tau_{LR_{1(2)}d_1\sigma}(\varepsilon) + \tau_{LR_{1(2)}d_2\sigma}(\varepsilon)$, and $\tau_{LR_{1(2)}\sigma} = \tau_{R_{1(2)}Ld_{1(2)}\sigma} + \tau_{R_{1(2)}LR_{2(1)}\sigma}$. Figures 3(a)–3(c) show the spin-dependent electric currents flowing from electrodes R_1, R_2, and L into the center QD region, respectively, with a temperature gradient $k_B\Delta T = 0.2$. The spin accumulation $\Delta n_{1(2)} = n_{1(2)\uparrow} - n_{1(2)\downarrow}$ in each QD is displayed in Fig. 3(d). Owing to the existence

of the intra-dot Coulomb interactions, the current and the spin accumulation show oscillation behaviors with the energy level ε_d. Different from the electric-bias-induced currents,[11] both the magnitude and the sign of the electric current, and the spin accumulation induced by the temperature gradient can be modulated by the gate voltage. The positive and the negative maxima emerge on both sides of the two Coulomb peaks at $\varepsilon_d = 0$ and $\varepsilon_d = -U$. From Eqs. (22) and (23), we can derive an approximate expression. Taking $J_{R_1\uparrow}$ as an example, a similar analysis can be employed for other electric currents. Using the Sommerfeld expansion,[27] we obtain

$$J_{R_1\uparrow} \simeq \frac{e\pi^2 k_B^2 T\Delta T}{3h}\tau'_{LR_1\uparrow}|_{\varepsilon=\mu}. \tag{24}$$

Though the above equation is applicable in the low-temperature region, we still capture some useful information. For example, the sign of $J_{R_1\uparrow}$ is determined by ΔT and $\tau'_{LR_1\uparrow}|_{\varepsilon=\mu}$, and thus it provides two methods to control the sign of the current. In Fig. (a), we show $\tau_{LR_1\uparrow}$ as a function of the incident electron energy near the Fermi levels at different energy levels. When the peak of $\tau_{LR_1\uparrow}$ is below the Fermi levels, $J_{R_1\uparrow}$ has a positive value due to $\tau'_{LR_1\uparrow} > 0$. When the peak of $\tau_{LR_1\uparrow}$ is above the Fermi levels, $J_{R_1\uparrow}$ becomes negative. However, $J_{R_1\uparrow}$ is zero when the peak of $\tau_{LR_1\uparrow}$ is aligned with the Fermi levels. Therefore, we can determine the location of the peak of the transmission probability with respect to the Fermi levels by the sign of the electric current. This information cannot be extracted for the electric-bias-induced case. Due to the conservation of the particle number and the same temperature gradient between the left and the right electrodes, the spin-up (down) current through one of the two right electrodes is identical with the spin-down (up) current through the other of the two right electrodes, namely, $J_{R_1\downarrow} = J_{R_2\uparrow}$ and $J_{R_1\uparrow} = J_{R_2\downarrow}$. The electric current flowing into the center QD region from the left electrode is unpolarized due to $J_{L\uparrow} = J_{L\downarrow}$. The above results can be well explained by the electronic transmission probabilities for different electrodes. In Figs. 4(b)–4(d), we show the corresponding electronic transmission probability as a function of the electron incident energy for $\varepsilon_d = 0$. From the numerical results, we clearly see the relations $\tau_{R_1L\uparrow} = \tau_{LR_1\uparrow} = \tau_{LR_2\downarrow}$, $\tau_{R_2L\uparrow} = \tau_{LR_1\downarrow} = \tau_{LR_2\uparrow}$, and $\tau_{R_{1(2)}L\uparrow} = \tau_{R_{1(2)}L\downarrow}$. These relations are in good agreement with the conservation law and can give a good interpretation of the numerical results in Fig. 3. In addition, since $\tau_{LR_{1(2)}\uparrow(\downarrow)}$ is smaller than $\tau_{LR_{1(2)}\downarrow(\uparrow)}$ in the whole energy region, $J_{R_{1(2)}\uparrow(\downarrow)}$ has a lower value than $J_{R_{1(2)}\downarrow(\uparrow)}$. Actually, the spin-polarized currents in the right electrodes originate from the quantum interference effects between two different paths of the electrons from the left electrode to the right electrode. If the RSOI is involved, the electrons with different spin components will pick up different phases when they tunnel between the two right electrodes. For the left electrode, there are four different paths from the right two electrodes to the left electrode, the spin-dependent information is exactly swallowed ($T_{R_1} = T_{R_2}$). Therefore, we find an unpolarized current through the left electrode.

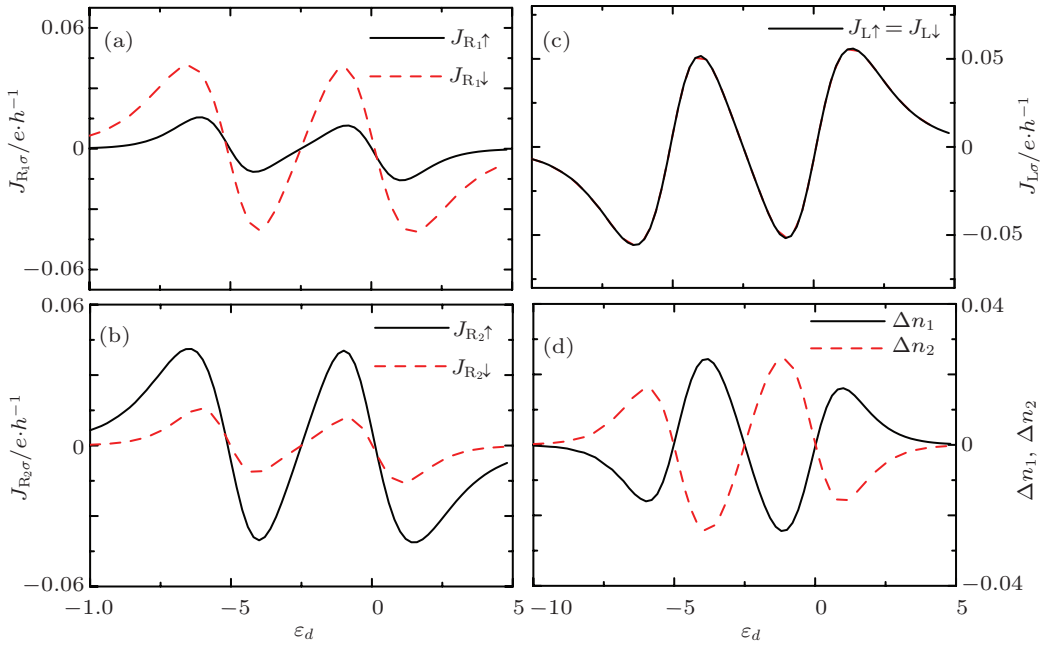


Fig. 3. (color online) Spin-polarized current and spin accumulation induced by the temperature gradient: (a) $J_{R_1\sigma}$, (b) $J_{R_2\sigma}$, (c)$J_{L\sigma}$, and (d) Δn_i $(i = 1,2)$ as functions of ε_d for $k_B\Delta T = 0.2$ and $k_B T = 0.5$. The other parameters are $k_B\varphi_R = 0.5\pi$, $\rho = 1$, and $U = 5$.

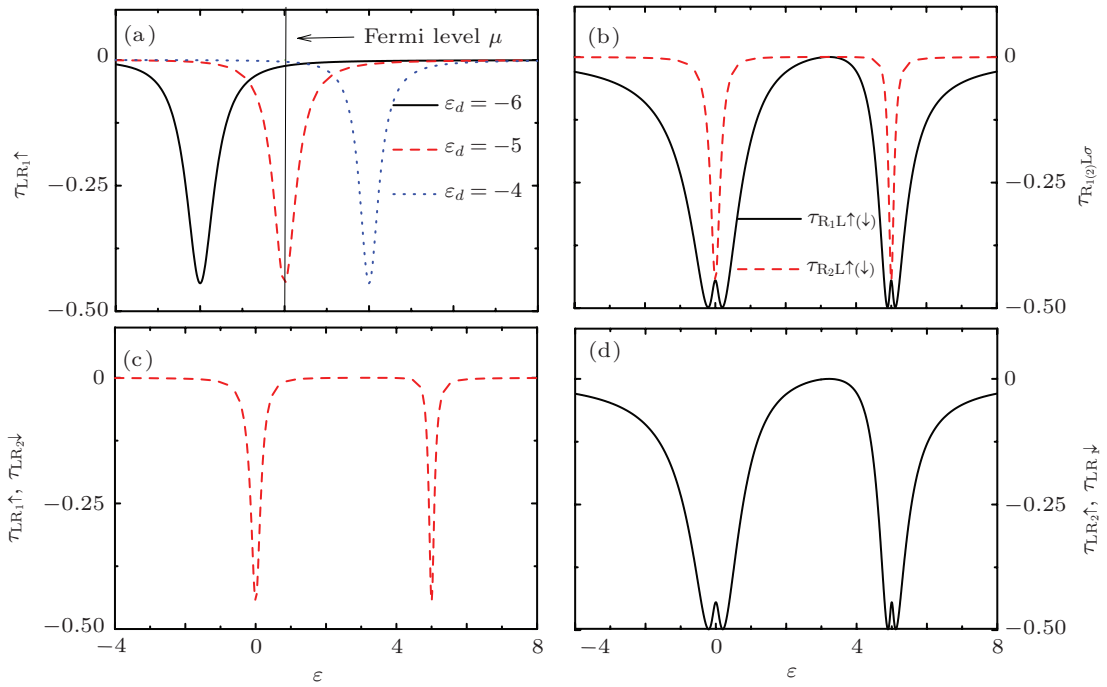


Fig. 4. (color online) Electronic transmission probabilities through the electrodes: (a) $\tau_{\mathrm{LR_1}\uparrow}$ as a function of the incident electron energy at different energy levels; (b) $\tau_{\mathrm{R_1L}\sigma}$, (c) $\tau_{\mathrm{LR}_{1(2)}\uparrow(\downarrow)}$, and (d) $\tau_{\mathrm{LR}_{1(2)}\downarrow(\uparrow)}$ (defined by Eqs. (16) and (17)) as functions of the incident electron energy for $\varepsilon_d = 0$. Other parameters are the same as those in Fig. 3.

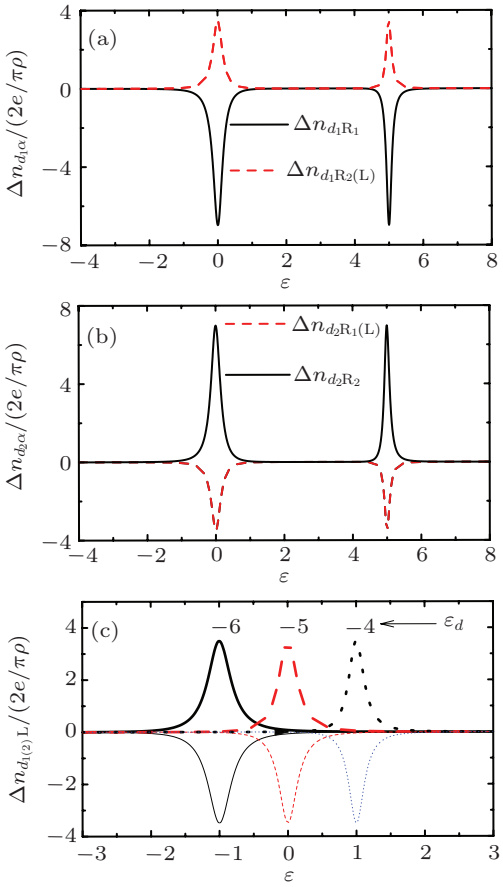


Fig. 5. (color online) The (a) $\Delta n_{d_1\alpha}$ and (b) $\Delta n_{d_2\alpha}$ as functions of the incident electron energy for $\varepsilon_d = 0$; (c) $\Delta n_{d_1\mathrm{L}}$ (thick lines) and $\Delta n_{d_2\mathrm{L}}$ (thin lines) as functions of the incident electron energy in the region near the Fermi levels. Other parameters are the same as those in Fig. 3.

Now we turn to study the spin accumulation on the QDs in the presence of a temperature gradient. By combining Eqs. (8)–(12), the electron occupation number with spin σ in each QD can be solved as

$$\langle n_{n\sigma}\rangle = \frac{2e}{\pi\rho}\int \mathrm{d}\varepsilon \sum_{\alpha} f_{\alpha}(\varepsilon)|G^{\mathrm{r}}_{d_n\alpha\sigma}(\varepsilon)|^2. \tag{25}$$

The intra-dot Coulomb interactions introduce many problems to the above equation, because the retarded Green's functions contain $\langle n_{j\sigma}\rangle$. A simple interpretation can be found in Ref. [11], while the information from the electrodes is not directly displayed. The spin accumulation in the j-th QD is defined as

$$\Delta n_j = \langle n_{j\uparrow}\rangle - \langle n_{j\downarrow}\rangle = \int \mathrm{d}\varepsilon \sum_{\alpha} f_{\alpha}(\varepsilon)\Delta n_{d_j\alpha}(\varepsilon), \tag{26}$$

where $\Delta n_{d_j\alpha} = \frac{2e}{\pi\rho}(|G^{\mathrm{r}}_{d_j\alpha\uparrow}(\varepsilon)|^2 - |G^{\mathrm{r}}_{d_j\alpha\downarrow}(\varepsilon)|^2)$ is the contribution to the spin accumulation in the j-th QD from electrode α. In the present case, we have the relations $\Delta n_{d_1\mathrm{R_1}} = -2\Delta n_{d_1\mathrm{R}_{2(\mathrm{L})}}$, $\Delta n_{d_2\mathrm{R_2}} = -2\Delta n_{d_2\mathrm{R}_{1(\mathrm{L})}}$, and $\Delta n_{d_1\mathrm{R_1}} = -\Delta n_{d_2\mathrm{R_2}}$ (see Figs. 5(a) and 5(b)). Therefore, equation (26) can be written as

$$\Delta n_{1(2)} = \int \mathrm{d}\varepsilon(f_{\mathrm{L}}(\varepsilon) + f_{\mathrm{R}_{2(1)}}(\varepsilon) - 2f_{\mathrm{R}_{1(2)}}(\varepsilon))\Delta n_{d_{1(2)}\mathrm{L}}. \tag{27}$$

Using the above equation, we can give a good interpretation of the spin accumulations on the QD induced by the temperature gradients. As shown in Fig. 3(d), both the sign and the magnitude of the spin accumulation can be modified in a controllable way by the gate voltage. To study the reason, an approximate

expression for the spin accumulation in the low-temperature region is given as

$$\Delta n_{1(2)} \simeq \frac{2e\pi^2 k_{\rm B}^2 T \Delta T}{3h} \Delta n'_{d_{1(2)}{\rm L}}|_{\varepsilon=\mu}. \tag{28}$$

This simple equation clearly shows that $\Delta n_{1(2)}$ can be determined by T, ΔT, and the slope of $\Delta n_{d_{1(2)}{\rm L}}$ at the Fermi levels. When T and ΔT are fixed, the sign and the magnitude of the spin accumulation are only determined by the slope of $\Delta n_{d_{1(2)}{\rm L}}$ at the Fermi levels (see Fig. 5(c)). From Fig. 3(d), we clearly see that the spin accumulations on the two QDs have the relation $\Delta n_1 = -\Delta n_2$, which arises from $\Delta n'_{d_1{\rm L}} = -\Delta n'_{d_2{\rm L}}$.

The corresponding spin-polarization efficiency of the electric current flowing into electrode ${\rm R}_i$ is plotted in Fig. 6. The spin-polarization efficiency is defined as $P_{{\rm R}_i} = (J_{{\rm R}_i\uparrow} - J_{{\rm R}_i\downarrow})/(J_{{\rm R}_i\uparrow} + J_{{\rm R}_i\downarrow})$. Figure 6(a) shows that $P_{{\rm R}_1}$ can approach -100% due to $J_{{\rm R}_1\uparrow} \simeq 0$ and $J_{{\rm R}_1\downarrow} \neq 0$ in the non-resonant regimes ($\varepsilon_d \ll \mu$ or $\varepsilon_d \gg \mu$), and an inverse spin-polarization efficiency emerges in electrode ${\rm R}_2$. These results are similar to those in the electric-bias-induced spin-polarization case.[11] However, when the electronic states are located near the Fermi levels, we find that $P_{{\rm R}_i}$ can reach infinity. To reveal the reasons behind, the enlarged figures of $J_{{\rm R}_i\sigma}$ near the Coulomb-induced electronic state are shown in Figs. 6(b) and 6(d). These figures clearly show that $J_{{\rm R}_i\uparrow}$ and $J_{{\rm R}_i\downarrow}$ have different signs when ε_d is located in the region from point A to point B. The equation $J_{{\rm R}_i\uparrow} = -J_{{\rm R}_i\downarrow}$ is satisfied at a certain intra-dot energy level, which means an infinite spin-polarization efficiency and that a pure spin current can be obtained in some particular energy levels. Unfortunately, the pure spin current is very weak due to $J_{{\rm R}_i\sigma} \simeq 0$ (see Figs. 3(a) and 3(b)).

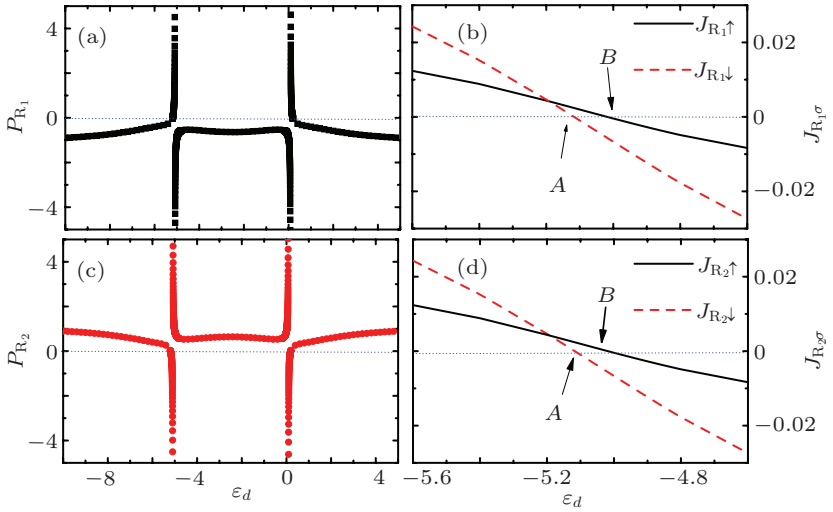


Fig. 6. (color online) The (a) $P_{{\rm R}_1}$ and (c) $P_{{\rm R}_2}$ as functions of ε_d. Panels (b) and (d) are the zoom-in plots of $J_{{\rm R}_1\sigma}$ and $J_{{\rm R}_2\sigma}$ in the energy region from -5.6 to -4.6. Other parameters are the same as those in Fig. 3.

We now show how to generate a large pure spin current by using the temperature gradient. As shown in Eq. (24), the sign of the spin-dependent electric current is determined not only by the slope of the transmission probability at the Fermi levels but also by the sign of the temperature difference between the electrodes. To obtain a large spin current, we fix the temperature of the left electrode at T, and raise (lower) the temperature of the right electrode ${\rm R}_2$ (${\rm R}_1$) by ΔT. Figure 7(a) shows charge current $J_{\rm LC}$ (in units of e) and spin current $J_{\rm LS}$ (in units of $\hbar$) through the left electrode, where we have defined the charge and the spin currents in electrode α as $J_{\alpha{\rm C}} = (J_{\alpha\uparrow} + J_{\alpha\downarrow})e$ and $J_{\alpha{\rm S}} = (J_{\alpha\uparrow} - J_{\alpha\downarrow})\hbar/2$, respectively.[49,50] Due to the existence of the intra-dot Coulomb interaction on each QD, the spin current has two positive and two negative maxima separately located on the two sides of the two Coulomb peaks $\varepsilon_d = 0$ and $\varepsilon_d = -U$. It is interesting to note that charge current $J_{\rm LC}$ becomes exactly zero when the intra-dot energy level is tuned to points A, B, C, D, E, and F as marked in Fig. 7(a), while the pure spin current has a large value at these points. We further find that the spin current has different signs at these points. This fact means that the pure spin current can be injected into or extracted out from the left electrode by the temperature gradients. Figure 7(b) shows $J_{\rm LC}$ as a function of $J_{\rm LS}$, and the points for obtaining a pure spin current are also marked in this figure. The positive (negative) maxima of the pure spin current in the left electrode can approach 0.06 (-0.06). In Figs. 7(c) and 7(d), we also show $J_{{\rm R}_1{\rm C}}$ ($J_{{\rm R}_2{\rm C}}$) as a function of $J_{{\rm R}_1{\rm S}}$ ($J_{{\rm R}_2{\rm S}}$). We find lower values of the positive (negative) maximum of the pure spin current in the right two electrodes.

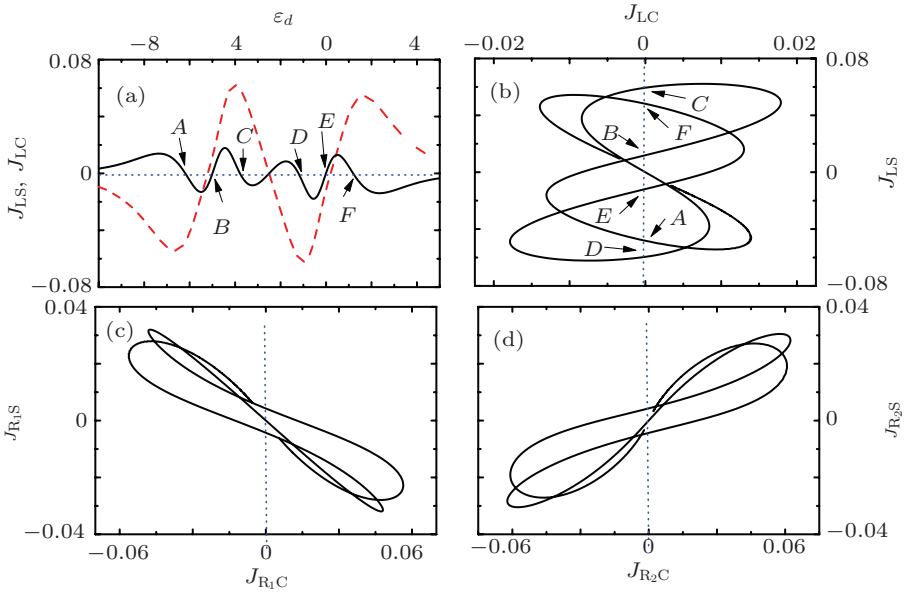


Fig. 7. (color online) The (a) J_{LC} (solid line) and J_{LS} (dashed line) as functions of ε_d; (b) J_{LC} as a function of J_{LS}; (c) J_{R_1C} as a function of J_{R_1S}; (d) J_{R_2C} as a function of J_{R_2S}. The temperature parameters are $k_BT = 0.5$ and $k_B\Delta T = 0.2$. Other parameters are the same as those in Fig. 3.

Finally, spin current J_{LS} and charge current J_{LC} as functions of $k_B\Delta T$ and k_BT are displayed in Figs. 8(a) and 8(c), respectively, where the location of the energy level is fixed at point F (see Fig. 7(a)). The corresponding spin accumulations on the QDs are plotted in Figs. 8(b) and 8(d). Figure 8(a) shows that the charge current is always close to zero, while the spin current has a linear behavior for $k_BT = 0.5$. A similar linear behavior can be observed for the spin accumulation on the QDs (see Fig. 8(b)). When the temperature gradient $k_B\Delta T$ is fixed at 0.2, J_{LC} and J_{LS} each have a linear behavior with the temperature of the left electrode k_BT in the low-temperature region. From Fig. 8(c), we clearly see that J_{LC} becomes zero when $k_BT \simeq 0.5$, while J_{LS} has a maximum at this temperature. The corresponding spin accumulations on the QDs have maximum values when k_BT is around 0.5 as shown in Fig. 8(d), and are suppressed with further increasing k_BT. The above results show that both the magnitude and the sign of the pure current can be controlled by the gate voltage and the temperatures of the electrodes.

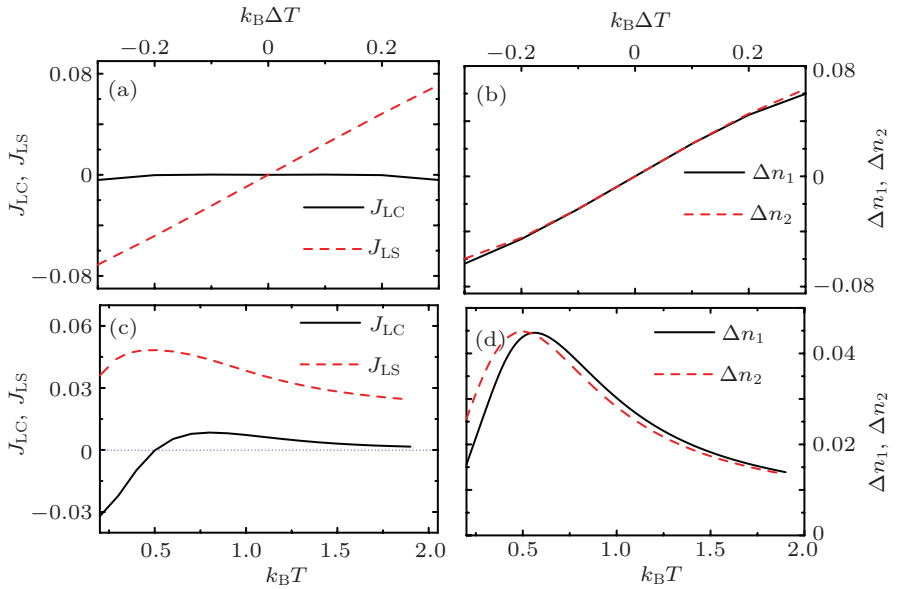


Fig. 8. (color online) The (a) J_{LC} (J_{LS}) and (b) spin accumulation on the QDs Δn_1 (Δn_2) as functions of $k_B\Delta T$; (c) J_{LC} (J_{LS}) and (d) Δn_1 (Δn_2) as functions of k_BT. The energy level ε_d is 1.2, and other parameters are the same as those in Fig. 3.

4. Summary

In conclusion, we have investigated the thermospin phenomena in a ring-shaped device consisting of two interacting QDs and three metallic electrodes. Our results show that both the sign and the magnitude of the spin-polarized current, and the spin accumulation on the QDs can be effectively controlled by adjusting the intra-dot energy levels and the temperature gradients. We also find that by properly adjusting the intra-dot energy levels, the temperature-induced spin-polarization efficiency in the electrodes can approach 100% (−100%), or even infinity, which indicates that a pure spin-up (down) current or a pure spin current can emerge in this thermal device.

References

[1] Vanderwiel W G, Franceschi S D, Elgerman J M, Tarucha S and Kouwenhoven L P 2002 *Rev. Mod. Phys.* **75** 1
[2] Žutić I, Fabian J and Sarma S D 2004 *Rev. Mod. Phys.* **76** 323
[3] Murayama A, Asahina T, Nishibayashi K, Souma I and Oka Y 2006 *Appl. Phys. Lett.* **88** 023114
[4] Hickey H C, Damsgarrd C D, Holmes S N, Farrer I, Jones G A C, Ritchie D A, Jacobsen C S, Hansen J B and Pepper M 2008 *Appl. Phys. Lett.* **92** 232101
[5] Datta S and Das S 1990 *Appl. Phys. Lett.* **56** 665
[6] Rashba E I 1960 *Fiz. Tverd Tela (Leningrad)* **2** 1224
[7] Bychkov Y A and Rashba E I 1984 *J. Phys. C* **17** 6039
[8] Hirsh J E 1999 *Phys. Rev. Lett.* **83** 1834
[9] Lü H F and Guo Y 1008 *Appl. Phys. Lett.* **92** 062109
[10] Chi F and Zheng J 2008 *Appl. Phys. Lett.* **92** 062106
[11] Chi F, Zheng J and Sun L L 2008 *Appl. Phys. Lett.* **92** 172104
[12] Chi F, Zheng J and Sun L L 2008 *J. Appl. Phys.* **104** 043707
[13] Gong W J, Zheng Y S and Lü T Q 2008 *Appl. Phys. Lett.* **92** 042104
[14] An X T, Mu H Y, Xian L F and Liu J J 2012 *Chin. Phys. B* **21** 077201
[15] Sánchez D and Serra L 2006 *Phys. Rev. B* **74** 153313
[16] Chen K W and Chang C R 2008 *Phys. Rev. B* **78** 235319
[17] Büttiker M, Imry Y, Landauer R and Pinhas S 1985 *Phys. Rev. B* **31** 6207
[18] Wesström J J 1999 *Phys. Rev. Lett.* **82** 2564
[19] Kwapiński T, Taranko R and Taranko E 2005 *Phys. Rev. B* **72** 125312
[20] Żak R A and Flensberg K 2008 *Phys. Rev. B* **77** 045329
[21] Ţolea M, Dinu I V and Aldea A 2009 *Phys. Rev. B* **79** 033306
[22] Liu Y S and Yang X F 2010 *J. Appl. Phys.* **108** 023710
[23] Liu Y S, Zhang D B, Yang X F and Feng J F 2011 *Nanotechnology* **22** 225201
[24] Wierzbicki M and Świrkowicz R 2011 *Phys. Rev. B* **84** 075410
[25] Karlström O, Linke H, Karlström G and Wacker A 2011 *Phys. Rev. B* **84** 113415
[26] Dubi Y and Di Ventra M 2011 *Rev. Mod. Phys.* **83** 131
[27] Liu Y S and Chen Y C 2009 *Phys. Rev. B* **79** 193101
[28] Liu Y S, Chen Y R and Chen Y C 2009 *ACS Nano* **3** 3497
[29] Uchida K, Takahashi S, Harii K, Ieda J, Koshibae W, Ando K, Maekawa S and Saitoh E 2008 *Nature* **455** 778
[30] Uchida K, Adachi H, An T, Ota T, Toda M, Hillebrands B, Maekawa S and Saitoh E 2011 *Nature Mater.* **10** 737
[31] Jaworski C M, Yang J, Mack S, Awschalom D D, Heremans J P and Myers R C 2010 *Nature Mater.* **9** 898
[32] Adachi H, Ohe J, Takahashi S and Maekawa S 2011 *Phys. Rev. B* **83** 094410
[33] Ohe J, Adachi H, Takahashi S and Maekawa S 2011 *Phys. Rev. B* **83** 115118
[34] Dubi Y and Di Ventra M 2009 *Phys. Rev. B* **79** 081302
[35] Hatami M, Bauer G W, Zhang Q F and Kelly P J 2009 *Phys. Rev. B* **79** 174426
[36] Świrkowicz R, Wierzbicki M and Barnaś J 2009 *Phys. Rev. B* **80** 195409
[37] Liu Y S, Chi F, Yang X F and Feng J F 2011 *J. Appl. Phys.* **109** 053712
[38] Liu Y S, Hong X K, Feng J F and Yang X F 2011 *Nanoscale Res. Lett.* **6** 618
[39] Qi F H, Ying Y B and Jin G J 2011 *Phys. Rev. B* **83** 075310
[40] Xue H J, Lü T Q, Zhang H C, Yin H T, Cui L and He Z L 2011 *Chin. Phys. B* **20** 027301
[41] Xue H J, Lü T Q, Zhang H C, Yin H T, Cui L and Z L He 2012 *Chin. Phys. B* **21** 037201
[42] Wang Q, Xie H Q, Jiao H J, Li Z J and Nie Y H 2012 *Chin. Phys. B* **21** 117310
[43] Trocha P and Barnaś J 2012 *Phys. Rev. B* **85** 085408
[44] Holleitner A W, Decker C R, Qin H, Eberl K and Blick R H 2001 *Phys. Rev. Lett.* **87** 256802
[45] Sun Q F, Wang J and Guo H 2005 *Phys. Rev. B* **71** 165310
[46] Nitta J, Akazaki T, Takayanagi H and Enoki T 1997 *Phys. Rev. Lett.* **78** 1335
[47] Mireles F and Kirczenow G 2001 *Phys. Rev. B* **64** 024426
[48] Haug H and Jauho A P 2007 *Quantum Kinetics in Transport and Optics of Semiconductors* (2nd edn.) (Berlin: Springer)
[49] Wang D K, Sun Q F and Guo H 2004 *Phys. Rev. B* **69** 205312
[50] Sun Q F, Guo H and Wang J 2003 *Phys. Rev. Lett.* **90** 258301